Computational and Theoretical Chemistry 1220 (2023) 113995

Contents lists available at ScienceDirect

Computational and Theoretical Chemistry

journal homepage: www.elsevier.com/locate/comptc

Adsorption behaviour of graphene, boron nitride and boron carbon nitride nanosheets towards pharmaceutical and personal care products

Shreyas S. Dindorkar [a], Raj Vardhan Patel [b], Anshul Yadav [b,*]

[a] Department of Chemistry, Jai Hind College, Mumbai 400020, India
[b] CSIR-Central Salt & Marine Chemicals Research Institute, Bhavnagar 364002, India

ARTICLE INFO

Keywords:
Graphene
Boron nitride
Boron carbon nitride
Adsorption
Triclosan
Triclocarban

ABSTRACT

Due to their toxic effects and the occurrence of triclosan and triclocarban (pharmaceutical and personal care products) in the water sources, there is an unmet need to remove them through a suitable method. In this study, the first principle density functional theory calculations were used to study and compare the adsorptive removal of triclosan and triclocarban using graphene, boron nitride, and boron carbon nitride nanosheets. The electrostatic potential maps, electron density distributions, density of states plots and molecular orbital distributions were obtained from the optimized structures. The electrostatic potential maps revealed that charge accretion takes place during the adsorption. The Van der Waals surfaces revealed that the graphene, boron nitride, and boron carbon nitride nanosheets exhibited several sites through which they can interact with triclosan and triclocarban. The thermodynamic feasibility of the process was evaluated by calculating the adsorption energy and the recovery time. The adsorption of triclosan and triclocarban molecules on the graphene nanosheet was exothermic, with an energy value of −28.5 kJ/mol and −18.9 kJ/mol, respectively. The non-covalent interaction isosurfaces and reduced density scatter plots were obtained to examine the weak interactions. The feasibility of adsorption followed the order graphene > boron carbon nitride > boron nitride.

1. Introduction

The consumption of pharmaceuticals and personal care products (PPCPs) has inevitably increased in everyday life due to the ever-increasing human population [1]. Active fungicides added to PPCPs threaten aquatic organisms and the quality of consumable water resources. As a result, residual fungicides are gaining attention as emerging pollutants and have become a serious concern due to their stability under natural environmental conditions [2]. Triclosan (TCS) and triclocarban (TCC) are efficacious and commonly exploited fungicides in PPCPs [3,4]. TCS is one of the most common organic contaminants found in water bodies in surface waters. At the same time, TCC is suspected of contaminating wastewater and surface water [3,4]. Due to their broad-spectrum use, TCS and TCC are frequently identified in seaweeds, snails, earthworms, drinking water and wastewater [5,6].

The limited consumable water resources on earth are negatively impacted by expanding industries and increased human activities in water-constrained areas [7]. The conventional processes in (waste) water treatment plants make it challenging to dispose of the TCS and TCC entirely. Consequently, laying down methods for effectively removing TCS and TCC from the marine ecosystem is very substantial. Researchers are presently using biodegradation, advanced oxidation and adsorption techniques to remove TCS and TCC from wastewater [8]. Due to its higher efficiency, the adsorption method is one of the widely used methods in wastewater treatment, which also has lower energy consumption. Hence, it is preferred for large-scale wastewater treatment operations [9]. Of course, adsorption has inherent flaws, such as low binding capacity, contamination brought about by leaking adsorbents into the water, and the difficulty in isolating adsorbents, which must be overcome [10,11]. Thus, it is necessary to design appropriate adsorbents with desired properties to remove TCS and TCC from the aqueous stream.

Recently, two-dimensional (2D) materials have emerged as strong candidates for removing new harmful chemicals from the environment [12]. In the last few decades, molybdenum disulphide [13], graphene (GRA) [14] and silicene [15] have been known for their intriguing features such as high surface area, optical transparency, low bandgap, flexibility, and high tensile strength. With the identification of graphene (GRA) as a potential adsorbent, many other nanosheets, such as boron nitride (BN), silicon carbide (SiC) and boron carbon nitride (BCN)

* Corresponding author.
E-mail address: anshuly@csmcri.res.in (A. Yadav).

https://doi.org/10.1016/j.comptc.2022.113995
Received 24 November 2022; Received in revised form 14 December 2022; Accepted 19 December 2022
Available online 20 December 2022

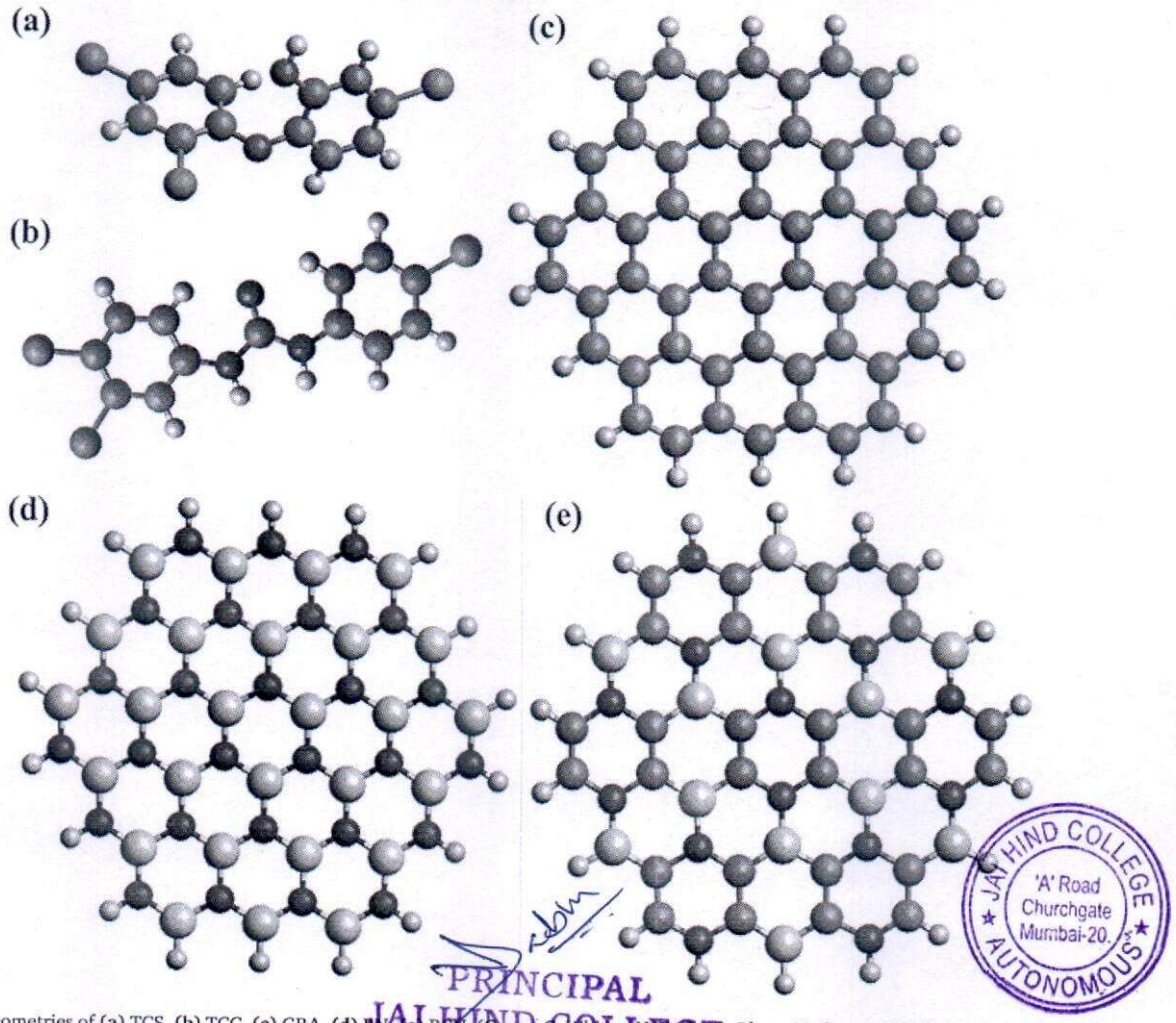

Fig. 1. Optimized geometries of (a) TCS, (b) TCC, (c) GRA, (d) BN, (e) BCN (Grey – C, White – H, Red – O, Blue – N, Green – Cl, Pink – B). (For interpretation of the references to colour in this figure legend, the reader is referred to the web version of this article.)

nanosheets, have generated attention [16–18]. For example, Li et al. [17] studied the interaction of bisphenol A and TCS with the graphene surface by varying different parameters, such as pH and ion concentration. The in situ synthesis of BN with N defects was reported by Zhu et al. [19] for the adsorptive removal of tetracycline. Xu et al. [20] reported that the TiO_2-BN composites show great efficiency for the photocatalytic oxidation of ibuprofen. Xing et al. [21] studied the effect of different solution conditions on the adsorption of ketoprofen, carbamazepine and bisphenol A by reduced graphene oxide, graphene, carbon nanotubes and powdered graphite.

Even though 2D materials have successfully removed the emerging pollutants that belong to the PPCPs compounds, their studies have not evolved significantly. Thus, there is scarce comparative information as to which 2D materials are more suitable for their adsorptive removal. Demonstrating the adsorption of TCC and TCS experimentally using all the nanosheets to arrive at the best among them can be tedious and complicated. One can use theoretical techniques as a pre-screening step to the conventional experimental techniques. The advantage of using theoretical methods is that it may help understand the interactions at the atomic level and save time, effort, and resources.

Against this backdrop, in this study, we report density functional theory (DFT) calculations based comparative study of monolayer GRA, BN, and BCN nanosheets towards the adsorption of TCS and TCC molecules from wastewater. The geometrical parameters are analyzed using the optimized geometries. Adsorption energy and recovery time were also calculated to gain insights into the thermodynamics of the interaction of TCS and TCC molecules on the nanosheets. The electrostatic potential maps, electron density distributions, the density of states (DOS), non-covalent interactions (NCI) isosurfaces and reduced density gradient (RDG) scatter plots were obtained. Different reactivity descriptors were also calculated based on the distribution and energies of the highest occupied molecular orbitals and lowest unoccupied molecular orbitals.

2. Computational details

The DFT calculations were performed in the Gaussian 09 software [22] to compute the TCS and TCC adsorption on the the GRA, BN, and BCN nanosheets each constituting 56 atoms. The BCN structure was chosen such that each carbon atom has nitrogen, carbon and a boron atom in its vicinity. Also, the stable C—C and B-N bonds were maximized. This contributed to the overall stability of the structure [23]. For periodic boundary conditions, the edge of GRA, BN, and BCN nanosheets were saturated with H atoms. To investigate the long-range corrections, a hybrid Coulomb-attenuated Becke-3-Lee-Yang-Parr (CAM-B3LYP) functional was utilized, combined with a polarizable continuum model (PCM) utilizing the integral equation formalism variant [24]. The CAM-B3LYP technique yields consistent and reliable findings for processes that need an atomistic knowledge of the interactions [25]. Thus, the CAM-B3LYP functional was used in the current work, which was corrected for dispersion adjustments using Grimme's D3 model and basis set superposition error using the counterpoise correction (BSSE) [26]. The 6-31G basis set was chosen in this study for the reasons mentioned in our earlier studies [27–29]. The following relationships were utilized

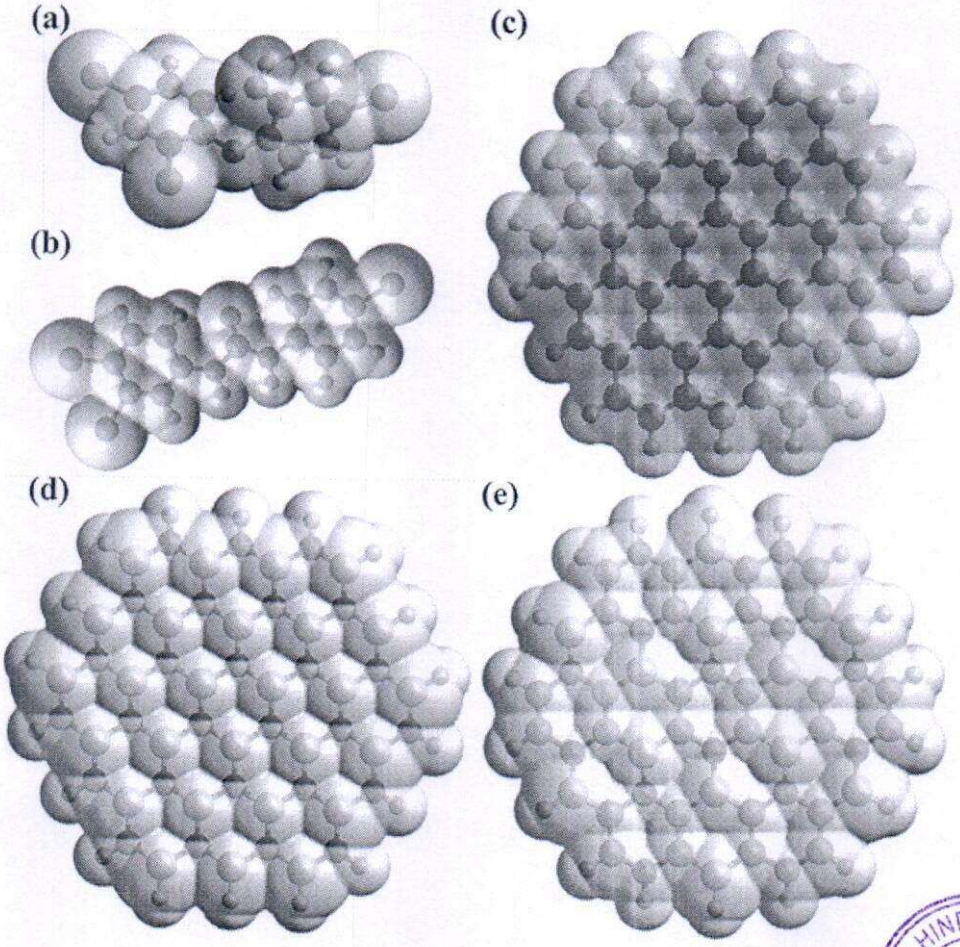

Fig. 2. Electrostatic potential maps of (a) TCS, (b) TCC, (c) GRA, (d) BN, (e) BCN.

to compute various reactivity descriptors.

$$ChemicalPotential(\mu) = -\frac{I+A}{2} \quad (1)$$

$$ChemicalHardness(\eta) = \frac{I-A}{2} \quad (2)$$

$$Electrophilicity(\omega) = \frac{\mu^2}{2\eta} \quad (3)$$

The terms I and A denote the negative of the HOMO ($I = -E_{HOMO}$) and the LUMO ($A = -E_{LUMO}$) energy, respectively. I and A refer to the ionization potential and the electron affinity of the molecules based on which the reactivity descriptors have been defined (Eqs (1) – (3)). The adsorption energy was estimated to determine the stability of the adsorption clusters. The following equation was used to calculate the adsorption energy.

$$E_{ads} = E_{sys} - (E_{adsorbent} + E_{adsorbate}) \quad (4)$$

where the term, E_{sys} represents the total energy of the complex clusters, $E_{adsorbent}$ is the energy of the optimized nanosheet and $E_{adsorbate}$ is the energy of the optimized TCS and TCC molecule. The recovery time (τ) was estimated using the Van't-Hoff-Arrhenius equation [30]

$$\tau = \nu_0^{-1} e^{\left(\frac{-E_{ads}}{K_T}\right)} \quad (5)$$

where ν_0, T and K_T are the attempt frequency (10^{12} s), temperature and Boltzmann constant, respectively.

2.1. Results and discussions

The optimized structures of TCC and TCC molecules shown in Fig. 1 (a, b) indicated that in TCC, both the benzylic rings were coplanar, whereas TCS exhibited a non-planar geometry and underwent free rotation where the benzene rings were linked to each other through N—C—N linkage. TCS and TCC molecules contained two connected unsaturated benzene rings. Moreover, the π conjugation present in the benzene rings was responsible for its typical aromatic character. A combined effect of all these factors contributed to the stability of the TCS and TCC molecules [31]. Fig. 1 (c-e) shows the DFT-optimized geometries of the adsorbents viz., GRA, BN, and BCN sheets. The C—C, C—N, C-B, and B-N bond lengths in BCN nanosheet were 1.42, 1.36, 1.47, and 1.44 Å. Correspondingly, they were 1.41 and 1.45 Å in GRA and BN nanosheets, for the C—C and B-N bonds, respectively [28].

The Van der Waals surface where a molecule could be conceived as interacting with other molecules for the BN, BCN, GRA nanosheets and, TCS, TCC molecules are shown in Fig. 2. The red colour denotes the negative potentials (electrophilic sites), whereas blue denotes the positive potential (nucleophilic sites). The Van der Waals surfaces revealed that the GRA, BN, and BCN nanosheets exhibited several sites through which they can interact with TCS and TCC. The BN and BCN nanosheets showed no positive or negative electrostatic potential. However, the GRA nanosheet showed an electronegative potential throughout the nanosheet, which can be due to the rich electron density of the graphene surface [32]. The H atoms in the vicinity of the electronegative chlorine and the oxygen atoms in TCS and TCC molecules showed electropositive potential on their surfaces, whereas the electronegative atoms exhibited an electronegative potential. The C atoms in TCS and TCC molecules

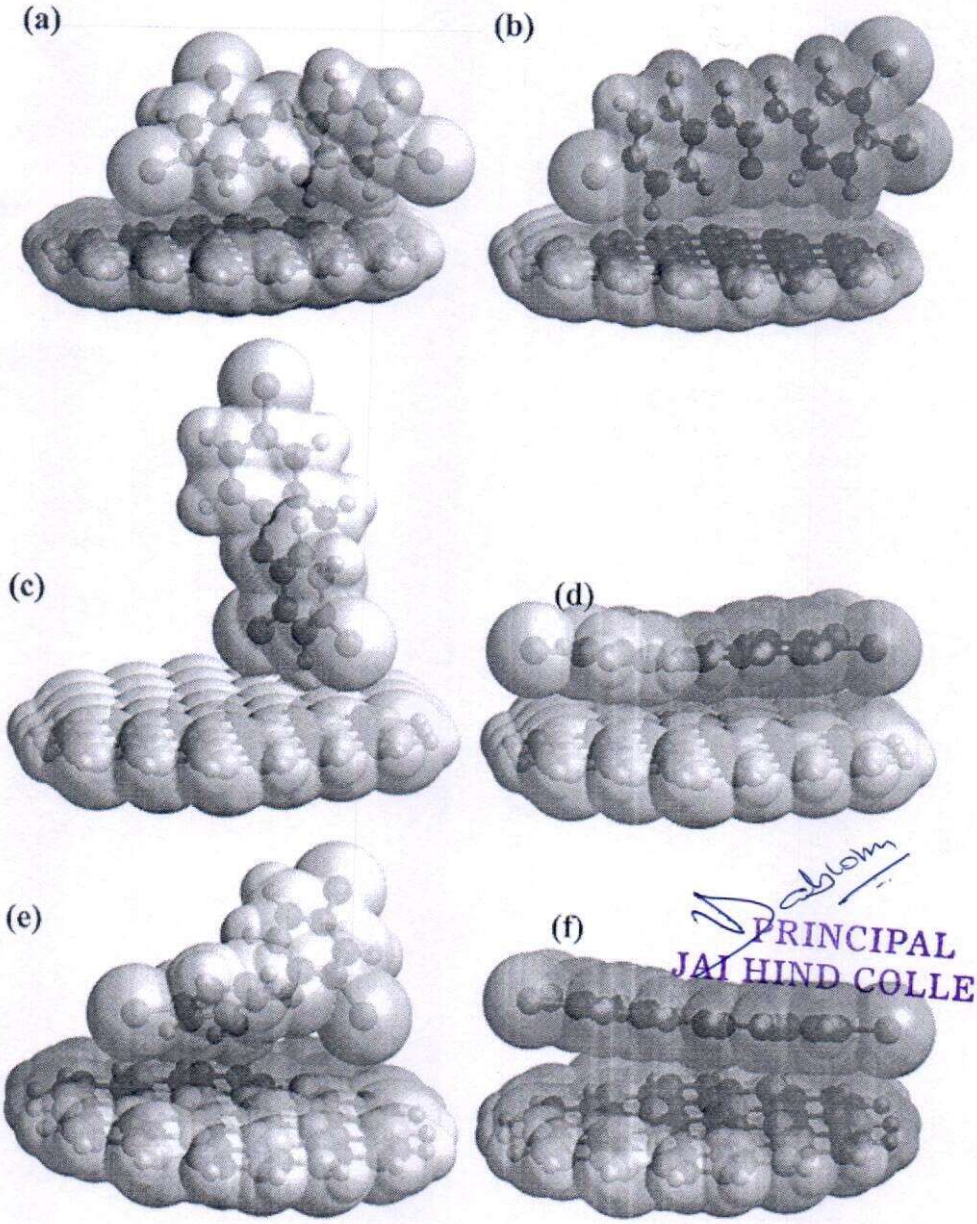

Fig. 3. Electrostatic potential maps of different clusters (a) TCS-GRA, (b) TCC-GRA, (c) TCS-BN, (d) TCC-BN, (e) TCS-BCN, (f) TCC-BCN.

were mostly in the region of the neutral potential.

Fig. 3 represents the Van der Waals surfaces and the electrostatic potential for the optimized geometries of TCS and TCC adsorbed on BN, BCN and the GRA nanosheets, respectively. Except for the case of TCS adsorbed on the BN nanosheet, other adsorption interactions led to the accretion of the charge in the vicinity of the interaction sites.

The electron density distributions of the interacting molecules (Fig. 4) revealed the density of electrons surrounding each atom in the BN, BCN, and GRA nanosheets and the adsorbate molecules, i.e., TCS and TCC. In the case of the BN and the BCN nanosheets, the electron density was maximum around the N atoms, attributed to its electronegative nature. The N atoms were followed by the C and the B atoms, respectively, in terms of the electron densities in the BCN nanosheet. The C atoms in the GRA nanosheet showed a highly dense distribution of electrons around them. This observation was in accordance with the reported electronic properties of GRA [33]. The electron density distributions of TCS and TCC molecules showed the distribution of electrons around the molecule's electronegative N, O and Cl atoms. The benzene rings in both molecules showed evidence of the electron distribution along the plane of the rings, although the distribution was less dense than those around the electronegative atoms.

The TCS and the TCC molecules were placed at different positions from the GRA, BN, and BCN nanosheets to obtain the system with the lowest energy (Fig. 5). The optimized geometries of TCS and TCC were oriented at different angles with different adsorbent nanosheets. TCC was oriented parallel to BN and BCN nanosheets. In the case of the GRA nanosheet, TCC was perpendicular to the plane of the GRA nanosheet, with the α-hydrogen (with respect to the chloro group) being closest to the nanosheet at a distance of 2.39 Å. The H atom, at the α position, with respect to the chlorine atoms, was oriented towards the BN nanosheet. The plane of the two benzene rings was perpendicular to the plane of the BN nanosheet and made an angle of 105° with each other. On the BCN nanosheet, the H atoms of the benzene ring of TCS with single chlorine attached to it faced the nanosheets. The electron-rich GRA nanosheet interacted with the TCS molecule through the H atoms bonded to the electronegative atoms (O, Cl). The closest distances of TCS and TCC molecules from the different nanosheets are included in Table 1. Based on the equilibrium positions of the optimized structures of the TCS and

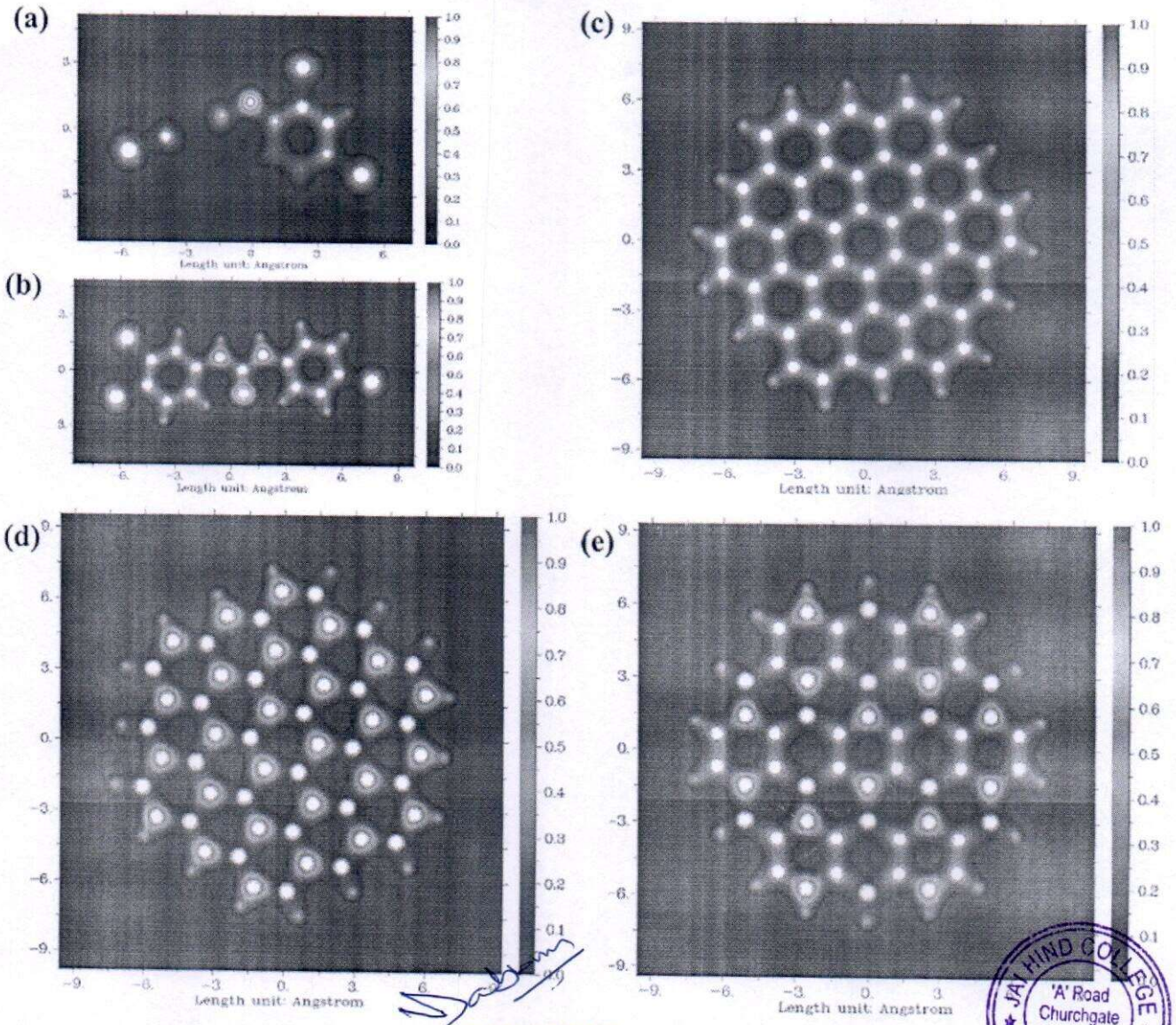

Fig. 4. Electron density distribution maps of (a) TCS, (b) TCC, (c) GRA, (d) BN, (e) BCN.

TCC, the closest approach of the TCS and the TCC was towards the GRA nanosheet. The shortest distance between the adsorbate and nanosheets was greater than 2 Å, indicating the physical nature of adsorption interactions [34].

The distribution of the highest occupied molecular orbitals (HOMO) and the lowest unoccupied molecular orbitals (LUMO) of the BN, BCN, GRA nanosheets and the TCS, TCC molecules are shown in Fig. 6 to examine the location of the possible interaction sites. In the case of BCN and BN nanosheets, the LUMOs resided on the electron-deficient B atoms, whereas the HOMOs resided on the C and N atoms in BCN and on electronegative N atoms in the BN nanosheet. TCS and TCC showed HOMOs around the electronegative atoms. This was attributed to the presence of the lone pairs on the atoms, and their nucleophilic character is also evident from the electrostatic potential maps. The HOMO and the LUMO distribution for the clusters of TCS and TCC adsorbed on GRA, BN, and BCN nanosheets are shown in Fig. 7.

To find the spacing of different energy levels and the energy gap between the HOMO and LUMO of the individual molecules and the clusters, the DOS plots were obtained (Fig. 8). The value of the energy gaps was evaluated based on the DOS plots. TCS and TCC showed a bandgap of 5.22 and 5.67 eV, respectively. The energy gaps of the BCN and GRA nanosheets did not change after the adsorption of TCS and TCC molecules. Nevertheless, in the BN nanosheet case, the bandgap's significant lowering was observed after the adsorption of TCS and TCC molecules. The band gap decreased after adsorption interaction due to the appearance of new energy levels at about −1 eV. The extent of lowering was greater in the TCS adsorbed cluster. This could have been because of the orientation at which TCS was in equilibrium after the adsorption.

The calculated reactivity descriptors values are shown in Table 2. The hardness of TCS and TCC is comparable, and the values are 7.39 eV and 7.04 eV, respectively. An increment in the chemical hardness was observed for both TCS and TCC after the adsorption on the GRA nanosheet. The GRA nanosheet made the adsorptive removal of TCS and TCC easier [35]. The post-adsorption hardness of TCS and TCC decreased slightly in the case of the BN and BCN nanosheets. The minimum electrophilicity principle suggests that the molecules tend to decrease their electrophilicity power during a chemical process, becoming less reactive [36]. The electrophilicity of the TCS and TCC molecules became the least after the adsorption on the GRA nanosheet (Table 2). The average electrophilicity value was −0.88 eV when TCS and TCC were adsorbed on the BN and BCN nanosheets. Furthermore, the chemical potential was around 4 eV for TCS and TCC when the adsorbent was GRA nanosheet. In the case of BN and BCN nanosheets, the average chemical potential

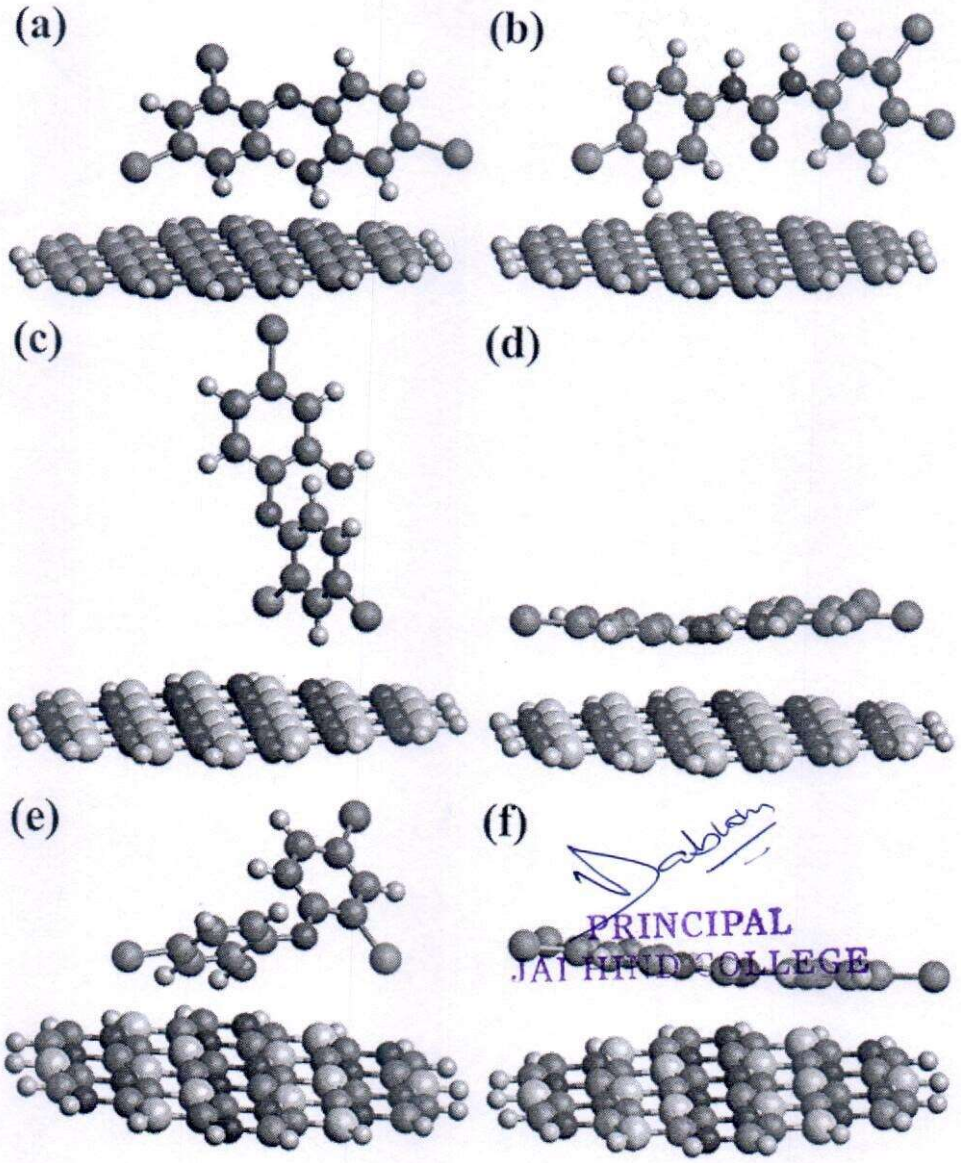

Fig. 5. Optimized geometries of different clusters (a) TCS-GRA, (b) TCC-GRA (c) TCS-BN, (d) TCC-BN, (e) TCS-BCN, (f) TCC-BCN. (Grey – C, White – H, Red – O, Blue – N, Green – Cl, Pink – B). (For interpretation of the references to colour in this figure legend, the reader is referred to the web version of this article.)

Table 1
Shortest distance of TCS and TCC from the GRA, BN, and BCN nanosheets.

	TCC			TCS		
	BN	BCN	GRA	BN	BCN	GRA
Closest atom	O	O	H	H	H	H
Shortest distance (Å)	2.95	3.21	2.39	2.48	2.25	2.13

was comparatively less (~3.5 eV). This led to a conclusion that among the three different nanosheets, GRA nanosheet was more favourable.

The adsorption energy for the TCS and TCC molecules adsorbed on the GRA, BN, and BCN nanosheets was evaluated to determine the nature of their interactions. The adsorption energies were −10.67 kJ/mol, −22.9 kJ/mol, and −28.46 kJ/mol for TCS when it was adsorbed on GRA, BN, and BCN nanosheets, respectively, and −7.58 kJ/mol, −11.96 kJ/mol, −18.96 kJ/mol for TCC adsorbed on GRA, BN, and BCN nanosheets, respectively. The negative sign indicated the feasibility of the reaction. It was evident that the adsorption of TCS and TCC molecules on the GRA nanosheet was comparatively more feasible than the other nanosheets. The recovery time for the adsorption of TCS was of the order of 0.1 ns, whereas for the TCC, the value was 0.16 ns. The faster recovery was due to the lower adsorption energies and suggested the reversible adsorption of TCS and TCC over GRA, BN, and BCN nanosheets. However, the recovery of TCS and TCC over the GRA and BCN nanosheets was comparatively slower by a few milliseconds. The analysis of thermodynamic parameters suggested that the chosen nanosheets are suitable for the adsorption of TCS compared to TCC. The results so obtained were sufficient to conclude that GRA acts as a better adsorbent for the adsorption of TCS and TCC molecules compared to BN and BCN nanosheets.

Fig. 9 represents the RDG scatter plots and the NCI isosurfaces of the adsorption clusters of TCS and TCC with GRA, BN, and BCN nanosheets. The NCI isosurfaces were coloured in green, which denotes the Van der Waals interactions; blue, which denotes the strong H bonding; red, denoting the steric repulsive interactions. The analysis showed that no significant weak interactions were observed in the GRA nanosheet. Instead, a small degree of intramolecular repulsive interactions was apparent in TCS and TCC molecules. The NCI isosurfaces of relaxed structures of TCS and TCC over BCN nanosheets showed the presence of weak interactions, which were due to the Van der Waals forces. Finally,

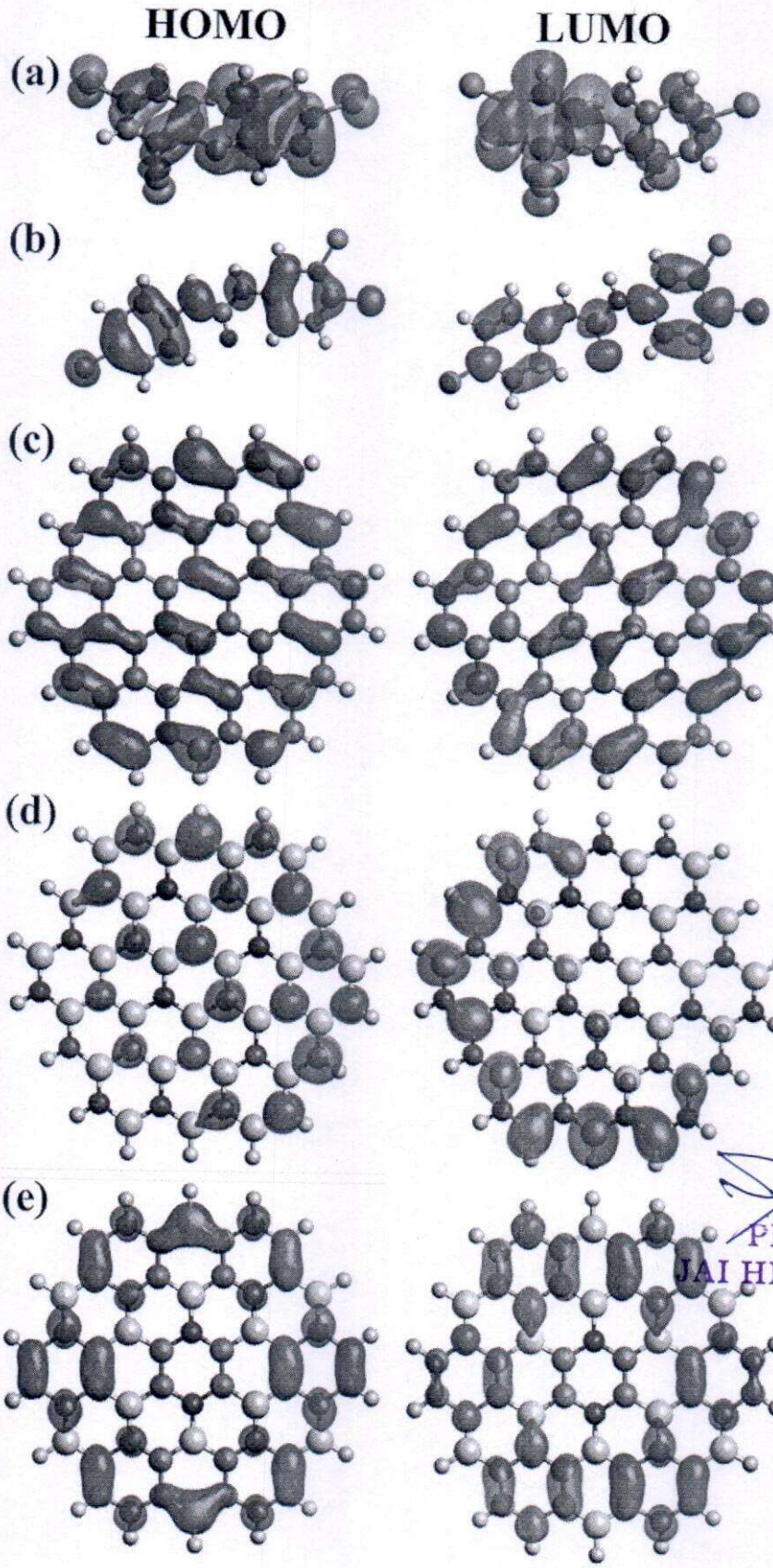

Fig. 6. HOMO and LUMO distribution for optimized structure of (a) TCS, (b) TCC, (c) GRA, (d) BN, (e) BCN.

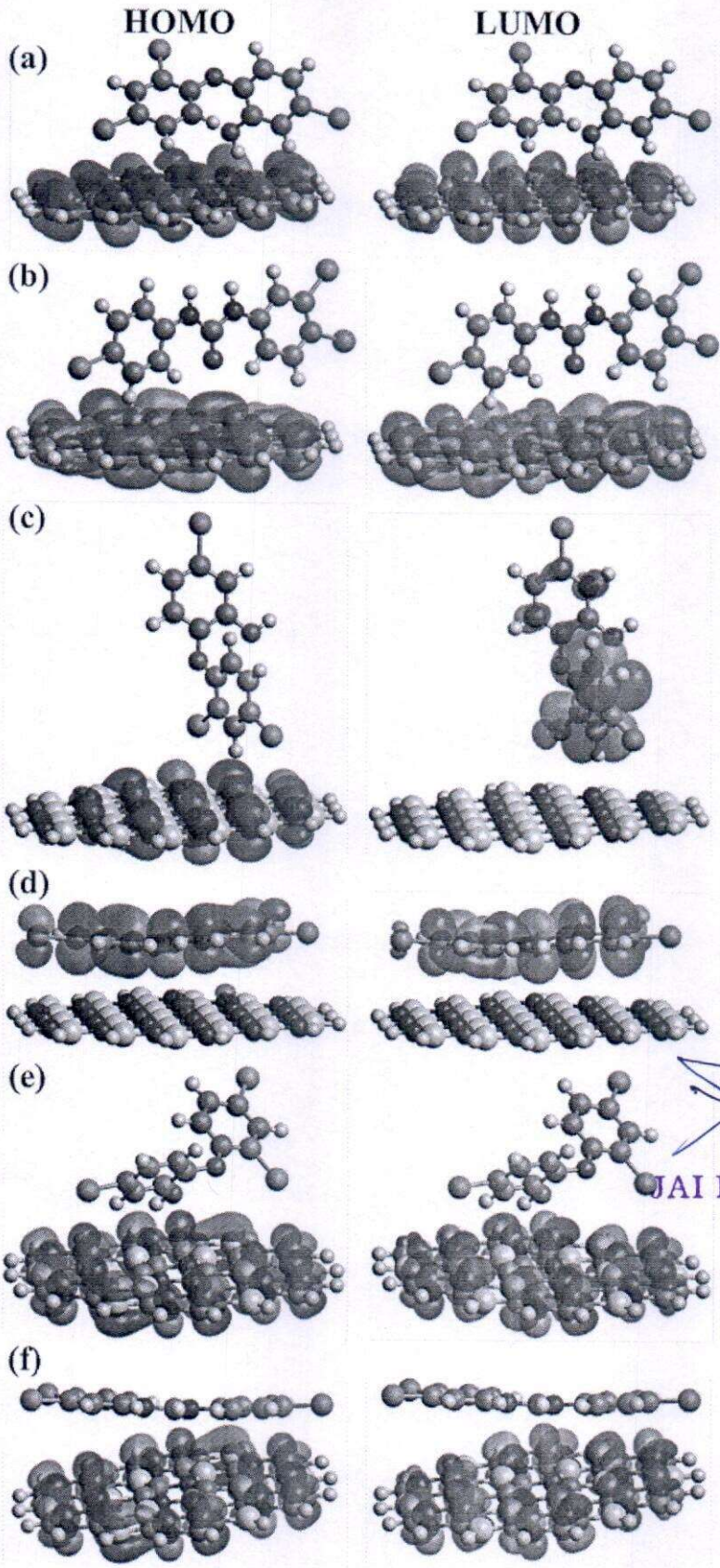

Fig. 7. HOMO and LUMO distribution for the optimized structure of different clusters (a) TCS-GRA, (b) TCC-GRA (c) TCS-BN, (d) TCC-BN, (e) TCS-BCN, (f) TCC-BCN.

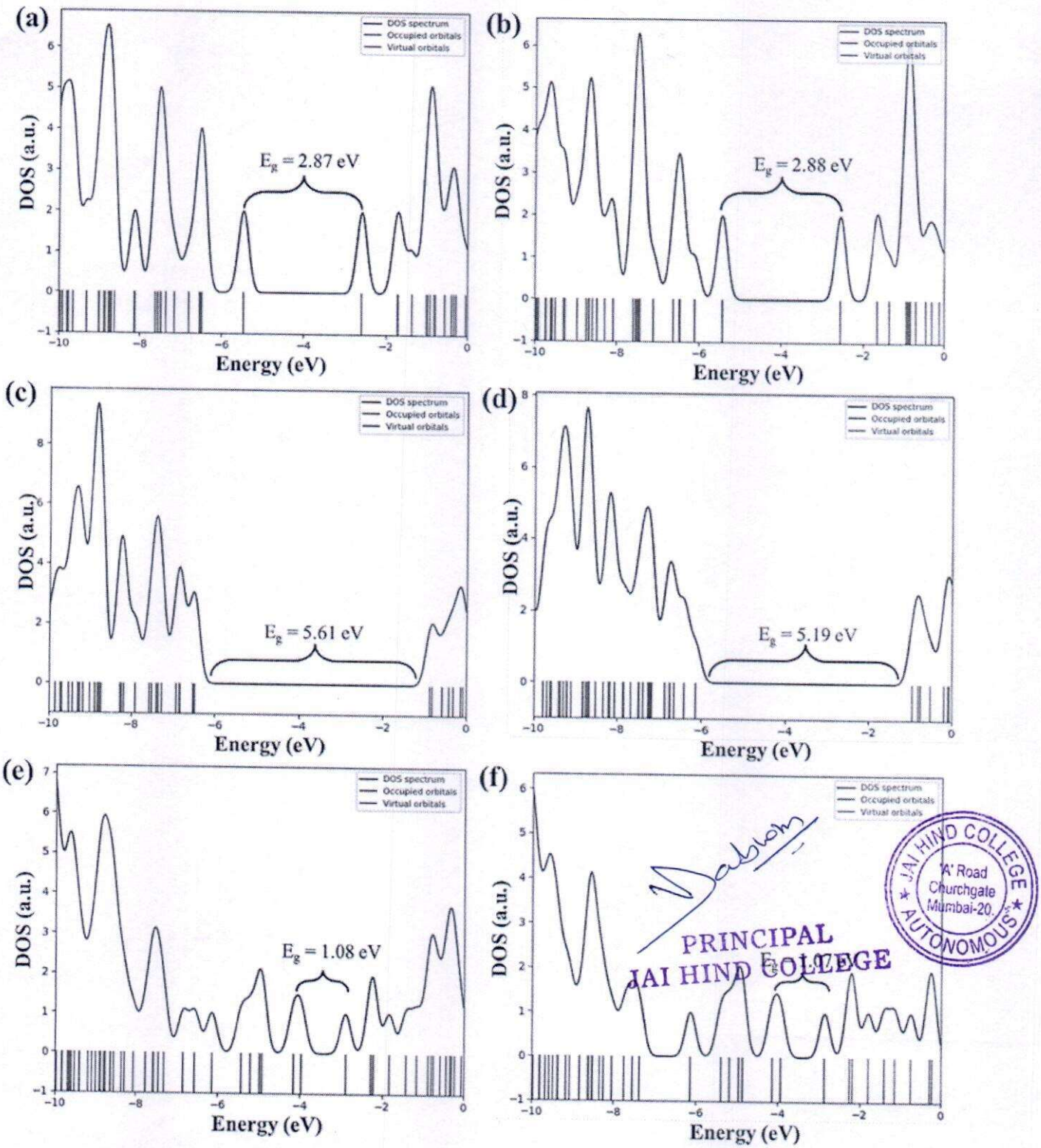

Fig. 8. DOS plots of different clusters (a) TCS-GRA, (b) TCC-GRA, (c) TCS-BN, (d) TCC-BN, (e) TCS-BCN, (f) TCC-BCN.

the clusters of TCS and TCC molecules with BN nanosheet showed the dominance of the Van der Waals interactions and were in line with the fact that the orientation of TCS and TCC was parallel to that of the BN nanosheet.

3. Conclusions

In this study, we investigated the adsorption of TCS and TCC molecules on GRA, BN, and BCN nanosheets using the first principle DFT calculations. The electrostatic potential maps and the electron density distributions for the molecules were obtained based on the optimized geometries. The GRA, BN, and BCN nanosheets showed electron densities around the more electronegative atoms. A similar observation was made in the case of TCS and TCC molecules. It was revealed from the electrostatic potential maps that charge accretion takes place during adsorption. The DOS plots obtained for evaluating the energy gaps of the

Table 2
Reactivity descriptors of the BN, BCN, GRA, TCS, and TCC cluster before and adsorption.

Parameters	BN	BCN	GRA	TCS	TCC	BN-TCS	BN-TCC	BCN-TCS	BCN-TCC	GRA-TCS	GRA-TCC
ΔE (kJ/mol)	–	–	–	–	–	−10.67	−7.58	−22.9	−11.96	−28.46	−18.96
HOMO (eV)	−6.48	−3.94	−2.51	−0.86	−0.91	−0.87	−0.94	−3.97	−3.9	−2.59	−2.55
LUMO (eV)	−0.13	−2.86	−5.4	−6.53	−6.13	−6.48	−6.13	−2.89	−2.83	−5.46	−5.43
HLG (eV)	6.35	1.08	2.89	5.67	5.22	5.61	5.19	1.08	1.07	2.87	2.88
Chemical Hardness (eV)	6.61	6.8	7.91	7.39	7.04	7.35	7.07	6.86	6.73	8.05	7.98
Chemical Potential (eV)	3.31	3.4	3.96	3.69	3.52	3.67	3.54	3.43	3.36	4.02	3.99
Electrophilicity (eV)	0.83	0.85	0.99	0.92	0.88	0.92	0.88	0.86	0.84	1.01	0.99

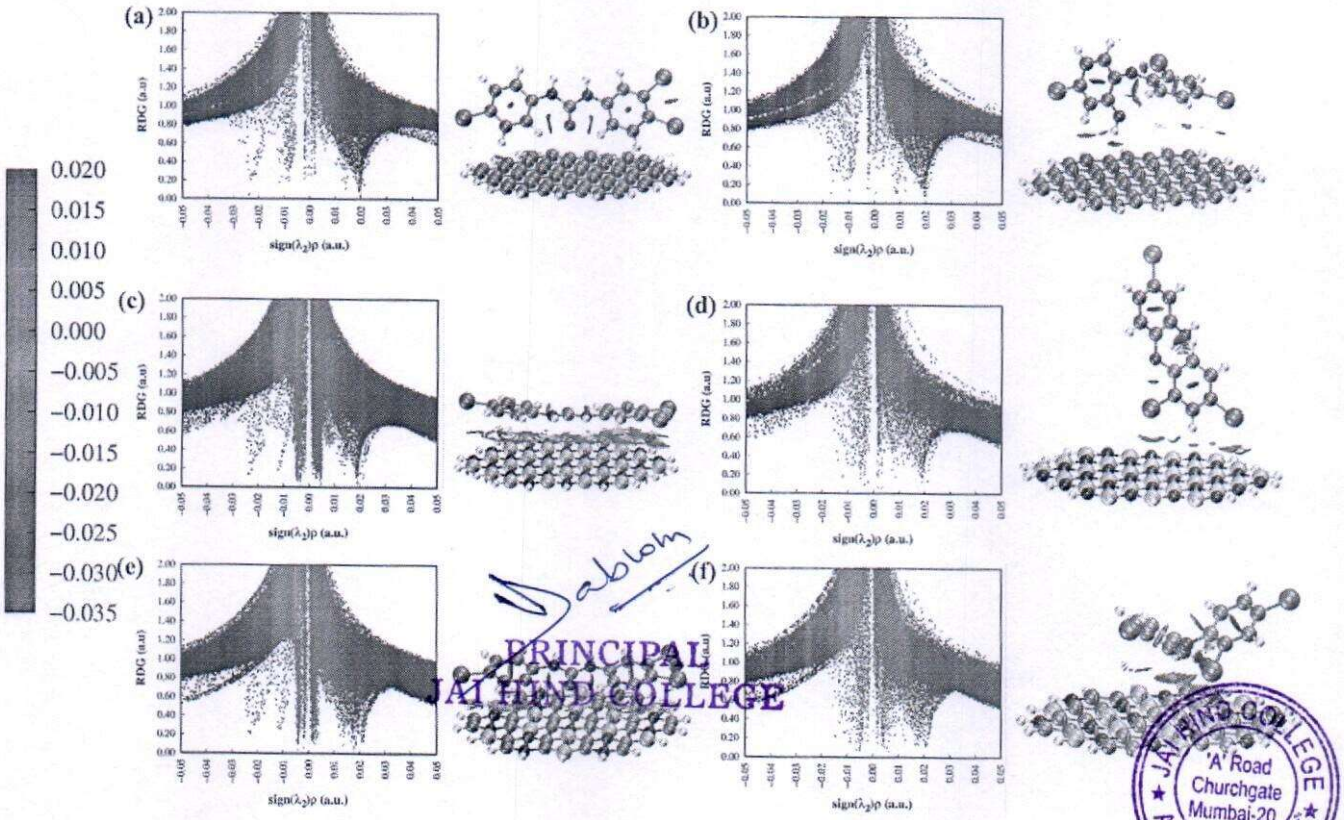

Fig. 9. RDG plots and NCI interactions in different clusters (a) TCS-GRA, (b) TCC-GRA (c) TCS-BN, (d) TCC-BN, (e) TCS-BCN, (f) TCC-BCN.

molecules showed that BCN has the lowest bandgap of 1.08 eV. However, when the reactivity descriptors were evaluated using Koopmans' theorem, favourable results were obtained for the GRA nanosheet. Adsorption energies and the recovery time values indicated that the interactions were weak and reversible. RDG scatter plots and the NCI isosurfaces showed that the Van der Waals forces mainly governed the interactions. The results showed that the adsorption of TCS and TCC molecules is more favourable on the GRA nanosheet.

CRediT authorship contribution statement

Shreyas S. Dindorkar: Methodology, Data curation, Visualization, Writing – original draft. **Raj Vardhan Patel:** Methodology, Data curation, Visualization, Writing – original draft. **Anshul Yadav:** Conceptualization, Methodology, Data curation, Visualization, Investigation, Writing – original draft, Writing – review & editing.

Declaration of Competing Interest

The authors declare that they have no known competing financial interests or personal relationships that could have appeared to influence the work reported in this paper.

Data availability

Data will be made available on request.

Acknowledgements

The authors thank Dr B. Ganguly, CSIR–CSMCRI, Bhavnagar, for his help in theoretical calculations. The registration number of this manuscript is 064/2022.

References

[1] H. Pu, P. Tang, L. Zhao, Q. Sun, Y. Zhai, Z. Li, N. Gan, Y. Liu, X. Ren, H. Li, Preparation of a carboxymethyl β-cyclodextrin polymer and its rapid adsorption performance for basic fuchsin, RSC Adv. 10 (2020) 20905–20914, https://doi.org/10.1039/C9RA10797E.

[2] M. Patel, R. Kumar, K. Kishor, T. Mlsna, C.U. Pittman, D. Mohan, Pharmaceuticals of Emerging Concern in Aquatic Systems: Chemistry, Occurrence, Effects, and Removal Methods, Chem. Rev. 119 (2019) 3510–3673, https://doi.org/10.1021/acs.chemrev.8b00299.

[3] R.U. Halden, D.H. Paull, Co-Occurrence of Triclocarban and Triclosan in U.S. Water Resources, Sci. Technol. 39 (6) (2005) 1420–1426.

[4] D.W. Kolpin, E.T. Furlong, M.T. Meyer, E.M. Thurman, S.D. Zaugg, L.B. Barber, H. T. Buxton, Pharmaceuticals, Hormones, and Other Organic Wastewater Contaminants in U.S. Streams, 1999–2000: A National Reconnaissance, Environ. Sci. Technol. 36 (2002) 1202–1211. 10.1021/es011055j.

[5] M.A. Coogan, T.W. La Point, Snail bioaccumulation of triclocarban, triclosan, and methyltriclosan in a North Texas, USA, stream affected by wastewater treatment plant runoff, Environ. Toxicol. Chem. 27 (2008) 1788–1793, https://doi.org/10.1897/07-374.1.

[6] Y. Yang, Y.S. Ok, K.-H. Kim, E.E. Kwon, Y.F. Tsang, Occurrences and removal of pharmaceuticals and personal care products (PPCPs) in drinking water and water/sewage treatment plants: A review, Sci. Total Environ. 596–597 (2017) 303–320, https://doi.org/10.1016/j.scitotenv.2017.04.102.

[7] A. Yadav, P.D. Indurkar, Gas Sensor Applications in Water Quality Monitoring and Maintenance, Water Conserv. Sci. Eng. 6 (2021) 175–190, https://doi.org/10.1007/s41101-021-00108-x.

[8] W.T. Vieira, M.B. de Farias, M.P. Spaolonzi, M.G.C. da Silva, M.G.A. Vieira, Removal of endocrine disruptors in waters by adsorption, membrane filtration and biodegradation. A review, Environ. Chem. Lett. 18 (2020) 1113–1143, https://doi.org/10.1007/s10311-020-01000-1.

[9] S.A. Ansari, R. Kumar, M.A. Barakat, M.H. Cho, Simple and sustainable route for large scale fabrication of few layered molybdenum disulfide sheets towards superior adsorption of the hazardous organic pollutant, J. Mater. Sci. Mater. Electron. 29 (2018) 7792–7800, https://doi.org/10.1007/s10854-018-8777-x.

[10] T.-H. Chen, I. Popov, W. Kaveevivitchai, O.Š. Miljanić, Metal-Organic Frameworks: Rise of the Ligands, Chem. Mater. 26 (2014) 4322–4325, https://doi.org/10.1021/cm501657d.

[11] Z. Lu, M.P. Prange, P.V. Sushko, Tuning Electronic Properties of 2D Materials Using Metal Adsorbates: Cu at WTe 2 Edges, J. Phys. Chem. Lett. 12 (2021) 6596–6603, https://doi.org/10.1021/acs.jpclett.1c01617.

[12] J. Theerthagiri, S.J. Lee, K. Karuppasamy, S. Arulmani, S. Veeralakshmi, M. Ashokkumar, M.Y. Choi, Application of advanced materials in sonophotocatalytic processes for the remediation of environmental pollutants, J. Hazard. Mater. 412 (2021), 125245, https://doi.org/10.1016/j.jhazmat.2021.125245.

[13] Z. Liang, R. Shen, Y.H. Ng, P. Zhang, Q. Xiang, X. Li, A review on 2D MoS2 cocatalysts in photocatalytic H2 production, J. Mater. Sci. Technol. 56 (2020) 89–121, https://doi.org/10.1016/j.jmst.2020.04.032.

[14] A. Yadav, S.S. Dindorkar, S.B. Ramisetti, N. Sinha, Simultaneous adsorption of methylene blue and arsenic on graphene, boron nitride and boron carbon nitride nanosheets: Insights from molecular simulations, J. Water Process Eng. 46 (2022), https://doi.org/10.1016/j.jwpe.2022.102653.

[15] Q. Guo, J. Liu, C. Bai, N. Chen, L. Qu, 2D Silicene Nanosheets for High-Performance Zinc-Ion Hybrid Capacitor Application, ACS Nano 15 (2021) 16533–16541, https://doi.org/10.1021/acsnano.1c06104.

[16] A. Yadav, N. Sinha, Nanomaterial-based gas sensors: A review on experimental and theoretical studies, Mater. Express. 12 (2022) 1–33, https://doi.org/10.1166/mex.2022.2121.

[17] E.C. Anota, 2D boron nitride incorporating homonuclear boron bonds: stabilized in neutral, anionic and cationic charge, SN Appl. Sci. 4 (2022) 295, https://doi.org/10.1007/s42452-022-05180-z.

[18] S.S. Dindorkar, R.V. Patel, A. Yadav, Unravelling the interaction between boron nitride nanosheets and organic pesticides through density functional theory studies, Colloids Surfaces A Physicochem. Eng. Asp. 649 (2022), https://doi.org/10.1016/j.colsurfa.2022.129550.

[19] Y. Chao, J. Zhang, H. Li, P. Wu, X. Li, H. Chang, J. He, H. Wu, H. Li, W. Zhu, Synthesis of boron nitride nanosheets with N-defects for efficient tetracycline antibiotics adsorptive removal, Chem. Eng. J. 387 (2020), 124138, https://doi.org/10.1016/j.cej.2020.124138.

[20] L. Lin, W. Jiang, M. Bechelany, M. Nasr, J. Jarvis, T. Schaub, R.R. Sapkota, P. Miele, H. Wang, P. Xu, Adsorption and photocatalytic oxidation of ibuprofen using nanocomposites of TiO2 nanofibers combined with BN nanosheets: Degradation products and mechanisms, Chemosphere 220 (2019) 921–929, https://doi.org/10.1016/j.chemosphere.2018.12.184.

[21] F. Liu, J. Zhao, S. Wang, P. Du, B. Xing, Effects of Solution Chemistry on Adsorption of Selected Pharmaceuticals and Personal Care Products (PPCPs) by Graphenes and Carbon Nanotubes, Environ. Sci. Technol. 48 (2014) 13197–13206, https://doi.org/10.1021/es5034684.

[22] Wallingford CT, Gaussian, Inc., (2013).

[23] K. Yuge, Phase stability of boron carbon nitride in a heterographene structure: A first-principles study, Phys. Rev. B. 79 (2009), 144109, https://doi.org/10.1103/PhysRevB.79.144109.

[24] T. Yanai, D.P. Tew, N.C. Handy, A new hybrid exchange–correlation functional using the Coulomb-attenuating method (CAM-B3LYP), Chem. Phys. Lett. 393 (2004) 51–57, https://doi.org/10.1016/j.cplett.2004.06.011.

[25] Z.-L. Cai, M.J. Crossley, J.R. Reimers, R. Kobayashi, R.D. Amos, Density Functional Theory for Charge Transfer: The Nature of the N-Bands of Porphyrins and Chlorophylls Revealed through CAM-B3LYP, CASPT2, and SAC-CI Calculations, J. Phys. Chem. B. 110 (2006) 15624–15632, https://doi.org/10.1021/jp063376t.

[26] E. Caldeweyher, C. Bannwarth, S. Grimme, Extension of the D3 dispersion coefficient model, J. Chem. Phys. 147 (2017), 034112, https://doi.org/10.1063/1.4993215.

[27] S.S. Dindonkar, A. Yadav, Comparative study on adsorption behaviour of the monolayer graphene, boron nitride and silicon carbide hetero-sheets towards carbon monoxide, Comput, Theor. Chem. 1210 (2022) 310–320, https://doi.org/10.1016/j.comptc.2022.113676.

[28] S.S. Dindorkar, N. Sinha, A. Yadav, Comparative study on adsorption of volatile organic compounds on graphene, boron nitride and boron carbon nitride nanosheets, Solid State Commun. 359 (2023), 115021, https://doi.org/10.1016/j.ssc.2022.115021.

[29] A. Yadav, S.S. Dindorkar, Vacancy defects in monolayer boron carbon nitride for enhanced adsorption of paraben compounds from aqueous stream: A quantum chemical study, Surf. Sci. 723 (2022), https://doi.org/10.1016/j.susc.2022.122131.

[30] V.S. Anithaa, R. Suresh, A.V. Kuklin, S. Vijayakumar, Adsorption of volatile organic compounds on pristine and defected nanographene, Comput. Theor. Chem. 1211 (2022), 113664, https://doi.org/10.1016/j.comptc.2022.113664.

[31] I. Păușescu, M. Medeleanu, M. Ştefănescu, F. Peter, R. Pop, A DFT Study on the Stability and Aromaticity of Heterobenzenes Containing Group 15 Elements, Heteroat. Chem. 26 (2015) 206–214, https://doi.org/10.1002/hc.21250.

[32] S. Sarkar, E. Bekyarova, R.C. Haddon, Covalent chemistry in graphene electronics, Mater. Today. 15 (2012) 276–285, https://doi.org/10.1016/S1369-7021(12)70118-9.

[33] A.H. Castro Neto, F. Guinea, N.M.R. Peres, K.S. Novoselov, A.K. Geim, The electronic properties of graphene, Rev. Mod. Phys. 81 (2009) 109–162, https://doi.org/10.1103/RevModPhys.81.109.

[34] S. Kawai, A.S. Foster, T. Björkman, S. Nowakowska, J. Björk, F.F. Canova, L. H. Gade, T.A. Jung, E. Meyer, Van der Waals interactions and the limits of isolated atom models at interfaces, Nat. Commun. 7 (2016) 11559, https://doi.org/10.1038/ncomms11559.

[35] R.G. Pearson, Chemical hardness and density functional theory, J. Chem. Sci. 117 (2005) 369–377, https://doi.org/10.1007/BF02708340.

[36] J.L. Gázquez, A hardness and softness theory of bond energies and chemical reactivity, in: 1998: pp. 135–152. 10.1016/S1380-7323(98)80007-1.

PRINCIPAL
JAI HIND COLLEGE

JAI HIND COLLEGE 'A' Road Churchgate Mumbai-20. AUTONOMOUS